Dynamics of single-file transport through soft nanopores: a case study via DNA nanocompartment channels

Youdong Mao[1,2], Song Chang[1], and Qi Ouyang[1]

[1]*Department of Physics and Center for Theoretical Biology, Peking University, Beijing 100871, China*

[2]*National Center for Nanoscience and Technology, Beijing 100080, China*

Abstract

We study the effects of channel-particle interactions on microscopic nonequilibrium single-file transport through soft nanochannels. A dual switching criticality picture is suggested to describe the correlation of channel gating with particle transport. To establish the relation between microscopic criticality and macroscopic quantities, for example, bulk concentration of solute particles, we simulated the mean residence number of solute particle inside one channel as a function of its bulk concentration, based on a one-dimensional lattice model. We found that this behavior fit well to first-order Langmuir isotherm. Considering a system configuration resembling real experimental setup, we established phenomenological models based on the proposed dual criticality picture, to show how to correlate channel gating with single-file transport in DNA nanocompartment system. These numerical calculations were then used to reproduce our recent experimental results based on equilibrium measurements, and showed good consistence. The modeling showed how microscopic nonequilibrium processes lead to macroscopic equilibrium consequence. We finally discuss the limitation of this theoretical investigation and its possible improvements.

I. INTRODUCTION

Single-file transport of microscopic particles, including atoms, ions, molecules, and colloids, through nanochannels is significant to both fundamental biological processes and industrial applications [1, 2, 3, 4, 5, 6, 7, 8, 9, 10, 11, 12]. Many-body statistical properties of single-file transport have been documented in both general context [2, 3, 4, 5] and special cases [6, 7, 8, 9, 10, 11, 12]. Most of these works consider steady state flux through nanochannels determined by the concentration and potential gradient [2, 3, 4, 5, 6, 7, 8], and even nonequilibrium fluctuations [9], with neglecting the flexibility of channels. However, nonequilibrium single-file transport is missing with considering simultaneously conformational changes of nanochannels exserted by channel-particle interactions. In this study, we investigate theoretically the microscopic nonequilibrium single-file transport through flexible nanochannels, given that the channel-particle interactions have indispensable nonequilibrium effect on the microscopic process of permeation and gating. To achieve a comparison between theoretical prediction and experiments, we study this problem on a concrete instance, i.e., DNA nanocompartment channels. We expect that this study will be helpful to improve our understanding to other nanochannels. We claim that this theoretical paper is an extend detailed version of our recent Letter that addresses the same problem both theoretically and experimentally [45].

Studies on DNA in the last decade have extend DNA from genetic materials to generic materials [13, 14]. DNA has been used to assemble nanostructure [15], nanodevice [16, 17], and nanofabrication template [18, 19]. With the emergence of active DNA nanocompartment (ADNC), DNA channels resembling protein channels can be formed in two-dimensional

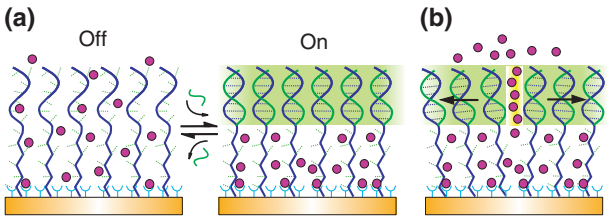

FIG. 1: (Color online) Idealized sketch of the DNA nanocompartment. (a) The on and off states of DNA nanocompartment. (b) Schematic illustration of the single-file transport of particles through a transient open channel.

assembly of double helix on solid substrates. The concept of reversibly switchable ADNC on surfaces is sketched in Fig. 1(a) [20, 21]. Single-stranded DNA (ssDNA) capped with a short piece of double-stranded DNA (dsDNA) can form a switching nanocompartment on gold surface by a compact array of DNA molecules. The high density packing of dsDNA caps and low density packing of ssDNA spacers establishes a nanometer height compartment. One major character of the ADNC is to switch between off and on states by hybridization (closing) and denaturation (opening). For a closed state ADNC with well-formed dsDNA membrane, experiments have shown that molecules with a size larger than 1 nm are impermeable through the dsDNA membrane at equilibrium states [21], because apertures between nearest neighbor molecules are in a diameter of about $\sim$ 1 nm. However, owing to the hydrophilicity of dsDNA molecules, small particles such as Na^+, K^+, Mg^{2+} and H_2O molecules are permeable through the dsDNA membrane. As the two-dimensional columnar assembly of dsDNA molecules in buffer solution is in a soft condensed matter form, each dsDNA molecule can have more motion freedom relative to solid condensed matter. This character can allow the intermolecular apertures to fluctuate between 1$\sim$3 nm, which may transiently form conducting channels with respect to the small particles with 1$\sim$2 nm size. In this theoretical contribution, we focus on this nontrivial non-equilibrium transport phenomena based on a dual-criticality picture.

In this paper we first investigate the thermodynamics of DNA channel deformation with analytic model, as presented in Section II. It forms the basis of stochastic dynamics of DNA channels, which is the key to its non-equilibrium transport phenomena. In Section III, we describe our proposed dual-criticality picture based on the stochastic dynamics of DNA channels. In this picture, we relate a single critical microscopic friction to two critical microscopic forces that cause non-equilibrium gating of DNA channels. To establish the relation between microscopic critical condition with macroscopic quantity, in Section IV, we simulate the mean residence number of transporter particles inside a channel as a function of the concentration gradient of the particles on the both side of a channel. The results fit much well to Langmiur isotherm that thermodynamically represents single-site binding model. This relation allows the two microscopic forces to determine two macroscopic concentrations. To apply the dual-criticality picture to solve a relatively real dynamic process corresponding to experimental system, in Section V, we establish a phenomenological analytical model to describe our recent experimental system, and numerically obtained the critical concentra-

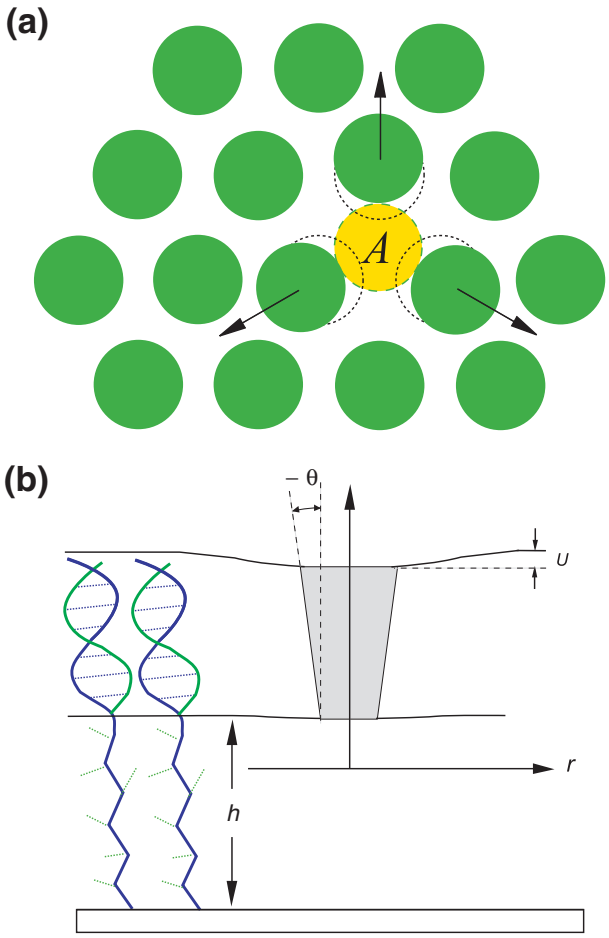

FIG. 2: (Color Online) The DNA channel and DNA membrane model. (a) Top view of a DNA channel that is dilated. (b) Side view of the DNA channel and its membrane. The decline mismatch U is the different between the channel thickness and the equilibrium DNA membrane thickness. We assume the surface of DNA membrane is normal to the orientation of DNA channel.

tions, which can well fit to experimental measurements. In the final Section of this paper, we discuss the limitation of this study, and further suggest the possible approaches to improve the dual-criticality picture and extend it to more widespread theoretical applications.

II. ANALYTIC MODEL FOR THE FREE ENERGY OF DNA CHANNEL

DNA channels formed in two-dimensional columnar assembly of dsDNA molecules, typically shown in Fig. 2, has complex conformational landscape, which depends on a large number of microscopic degrees of freedom that are analytically intractable. Although one could solve a precise conformational landscape by classical molecular dynamics, this does

not help with answering the problem of this study. We need to find a minimal model that captures the main characteristics of the DNA channels, based on which we can show complex coupling of channel gating with flux pumping. We consider that the Gibbs free energy of one DNA channel comprises three contributions: (1) the elastic energy between the dsDNA molecules that form the channel, which can be written as $\frac{1}{2}B(r-r_0)^2$, where r is the radius of the DNA channel, r_0 is the channel radius at original closed state, and B is the elastic modulus; (2) the potential caused by line tension along the edge of the channel, fL, where f is line tension, and L is the circumference of the channel; (3) the potential caused by area tension across the in-plane area of the channel, γA, where γ is the area tension, and A is the in-plane area. Therefore, the Gibbs free energy describing the deformation of the DNA channel is

$$U_C = \frac{1}{2}B(r-r_0)^2 + fL + \gamma A + U_0. \tag{1}$$

where U_0 is the absolute free energy when we remove all the three contributions.

The elastic modulus in the first item of Eq. (1) have two contributions. One contribution comes from the intermolecular interaction. The other comes from the ssDNA skeletons that immobilized on the surface, which acts like a pendulum in solution. Both of the contributions approximate the Hooke's law at second order. The former part can be asymptotically calculated from Kornyshev-Leikin theory [26, 27, 28, 29] for DNA interactions using $B_1 = \frac{\partial^2 U_{KL}(r=r_0)}{\partial r^2}$. The dsDNA membrane is in a electric field E originating from the repulsion of dsDNA membrane surface against the gold surface. The later part can be estimated by $B_2 = \sqrt{\frac{2\sigma E}{h}}$, where σ is the mean charge of each dsDNA molecule, and h is the height of the reservoir of the nanocompartment, i.e., the contour length of ssDNA skeleton.

The line tension in the second item of Eq. (1) is positive when the DNA channel is dilated. It also consists of two dominant contributions, thickness deformation and spontaneous curvature. The thickness deformation is induced by the conformational incline relative to the normal direction of the membrane surface. The thickness deformation energy is $G_1 = f_U \cdot 2\pi r = \frac{1}{2}KU^2 \cdot 2\pi r$, where K is an effective elastic modulus and is independent of DNA length, and U is half the conformational incline as defined in Fig. 2. The area of the part of the DNA membrane that is deformed by channel dilation is roughly equal to the circumference of the channel times an elastic decay length. The free energy induced by spontaneous curvature comes from locally increasing the curvature stress generated by

DNA columnar packing along its self-assembly surface. The radial dependent of this free energy is linear, because the effect is localized around the channel. Because the two side of the DNA membrane are asymmetric, with one side linked to solid surface, the spontaneous curvature of the top and bottom leaflets $C_{\pm}$ can be very different. It can work in terms of the composite spontaneous curvature of membrane near the channel, $C \equiv \frac{1}{2}(C_{+} - C_{-})$. The contribution of the deformation energy induced by spontaneous curvature is given by $G_2 = f_C \cdot 2\pi r = K_B C H' \cdot 2\pi r$, where H' is the midplane slope and K_B is the bending modulus, which roughly scales as the third power of the membrane thickness.

The area tension in the third item of Eq. (1) comes from the repulsive tendency of the DNA molecules surrounding the channel. When the channel is dilated, it causes the compression of the two-dimensional packing of the surrounding DNA molecules. This effect make the area tension is positive as the form written in Eq. (1).

After the rearrangement of these items, the Gibbs free energy of DNA channel deformation can be written explicitly in terms of the channel radius as

$$U_c(r) = \alpha \cdot \pi r^2 - f' \cdot 2\pi r + U_0' \tag{2}$$

where $\alpha = \frac{B}{2\pi} + \gamma$, $f' = \frac{B}{2\pi} r_0 - f$, and $U_0' = U_0 + \frac{1}{2} B r_0^2$. A free channel corresponds to the minimum energy of $U_c(r) = U_0' - \pi f'^2/\alpha$ with $r = f'/\alpha = r_0$. Similar representation recently has been used to analyze the gating of protein channels [25, 35]. However, the area tensions and line tensions in our case and in the case of protein channels have different sign. These treatment to the free energy of DNA channel deformation is borrowed from the elastic theory of lipid bilayer membrane [22, 25, 30, 35]. So this model is coarse-graining, which means that we neglect a few degrees of freedom that conformationally differ from the lipid bilayer membrane. However, it can help with a theory working analytically or semi-analytically.

III. DUAL CRITICALITY OF DNA CHANNEL GATING

In previous Section, we have established a coarse-graining model that can represent the free energy of channel deformation as a function of channel radius. This representation simplifies the dynamic analysis of channel switching under external perturbation. Mechanosensitive protein channels usually adopt a bistable conformational deformation energy [25, 34, 35]. Although its open state is triggered by external mechanical perturbation, the open state is

usually not considered sensitive to the pressure exerted by transporter particles. DNA channels in our model system of DNA nanocompartment have different characteristics. They have implications for a open state that is mechanically sensitive to interactions between channel and transporter particles. This effect could contribute more non-equilibrium effect on the channel gating.

Let us assume that the conformational stochastic dynamics between the open and closed states of a DNA channel can be described in terms of a one-dimensional reaction coordinate dynamics $x(t) = r - r_0$ in a conformational potential $U_c(x + r_0)$. The Fokker-Plank equation (FPE) for the probability density function (PDF) describing the channel dynamics under a external force $F(t)$ reads [34]

$$\frac{dp(x,t)}{dt} = D\partial_x \left(\partial_x + \beta \nabla_x \Phi(x,t)\right) p(x,t) \tag{3}$$

where $p(x,t)$ represents the PDF of finding the channel state in reaction coordinate x at time t, $\beta = 1/(k_B T)$, D is the diffusion coefficient of channel's conformational change, and $\Phi(x,t) = U_c(x + r_0) + F(t)x$. In the Smoluchowski approximation of FPE one assumes the functional form $p(x,t) = \sqrt{\alpha\beta}\exp\left[-\pi\alpha\beta(x - \langle x(t)\rangle)^2\right]$ [23]. Substituting it into Eq. (2), we derive

$$\frac{d\langle x(t)\rangle}{dt} = -\beta D(2\pi\alpha \langle x(t)\rangle - F(t)) \tag{4}$$

The exact solution of Eq. (3) for initial condition of $\langle x(0)\rangle = 0$ is

$$\langle x(t)\rangle = \beta D e^{-2\pi\alpha\beta D t} \int_0^t e^{2\pi\alpha\beta D t'} F(t') dt'. \tag{5}$$

If $F(t)$ takes a periodic function, it can be expanded in sinusoidal series $a\sum_{i=0}^{\infty} k_i \sin(\omega_i t + \phi_i)$. The exact solution of Eq. (3) then is $\langle x(t)\rangle = ce^{-2\pi\alpha\beta D t} + a\beta D \sum_{i=0}^{\infty} k_i \frac{2\pi\alpha\beta D \sin(\omega_i t+\phi_i) - \omega_i \cos(\omega_i t+\phi_i)}{(2\pi\alpha\beta D)^2+\omega_i^2}$, where c is determined by initial condition of $\langle x(0)\rangle = 0$. Figure 4(a) shows the mean trajectories of the DNA channel switching under special case of $F(t) = a\sin(\omega t)$. The behavior shows clear hysteresis, which can be quantified as

$$\langle H\rangle = \oint d\sin\omega t \cdot \langle x(t)\rangle = \frac{\pi a\beta D\omega}{(2\pi\alpha\beta D)^2 + \omega^2}. \tag{6}$$

The hysteresis has a maximum at $\omega = 2\pi\alpha\beta D$, as shown in Fig. 3(b). This means that very slow change and very fast change of external force $F(t)$ both decrease the degree of hysteresis.

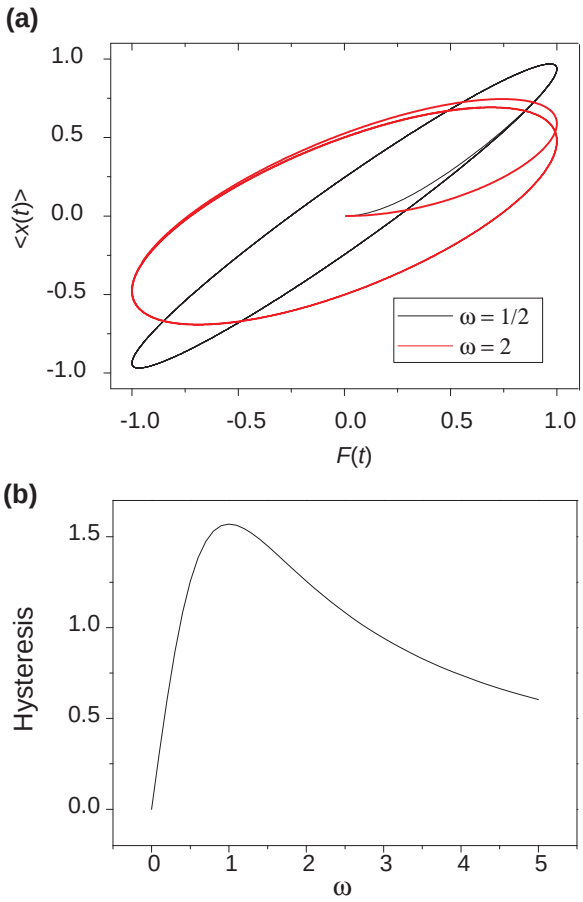

FIG. 3: (Color online) Mean trajectories of the DNA channel switching under external forcing $F(t) = a\sin(\omega t)$. Unit of $F(t)$ is set to a. (a) $F_+(t)$ and $F_-(t)$ are in symmetry. (b) The relation between hysteresis and ω. Parameters: $a = 2\pi\alpha = 6(\pi\beta)^{-1}$, D = 1.

Due the symmetry between ω and D in Eq. (6), the relation between the hysteresis and D is similar to Fig. 3(b).

Experiments have show that metal ions (Na^+, K^+) and water molecules can transport through a free DNA channel, which have a diameter estimated to be about 0.5$\sim$1 nm. It is trivial to study the transport behavior of these ions and molecules. We focus on the small particles with a radius r_p comparable to the radius r_0 of the free DNA channels, which can not transport through the free DNA channels at equilibrium state under low concentration gradient. To understand the switching of DNA channel with respect to these small particles, we have to clarify the interactions between DNA channels and particles.

Imagine the scenario that one solute particle with radius r_p resides right in the center of

the channel. The channel-particle interactions can be simulated by a steep-wall potential [32]

$$\Phi_{cp}(\rho) = \begin{cases} 4\epsilon \left[\left(\frac{\rho-\rho_0}{\sigma}\right)^{12} - \left(\frac{\rho-\rho_0}{\sigma}\right)^{6} \right] & \rho - \rho_0 > \sigma/\sqrt[6]{2} \\ 0 & \rho - \rho_0 \leq \sigma/\sqrt[6]{2}, \end{cases} \tag{7}$$

where ρ denotes the distance between the axis of the channel and the center of the solute particle, and $\rho_0 = r - r_c$, $r_c = \sigma + r_p$. We are aware that this potential is not exact. However, it was shown that simulation based on the potential can produce result agreeing with experimental observation of single-file diffusion across nanochannel [32]. According to Eq. (7), when $r < r_c$ the channel-particle interactions provide a sufficiently large friction that makes particle incapable of moving along the channel; when $r \geq r_c$ only a small viscous friction γ exists, allowing the particle to transport through the channel. We refer to r_c as critical radius or switching radius. Figure 4 illustrates the three cases for the conformation of DNA channel. The critical radius provide a microscopic mechanism for the transport behavior of solute particles across the DNA membrane.

Mapping the critical radius to the external force applied on DNA channel can show how $F(t)$ causes the switching of the DNA channel. As shown in Fig. 5, when the inside driving force $F(t)$ is large enough, the switching radius can exist in the range of radius variation, and it thereby determines two different critical forces, i.e., F_o causing the opening of the channel during the increasing phase ($F_+(t)$), and F_c causing the closing of the channel during the decreasing phase of ($F_-(t)$). For a dynamic hysteresis of the type as Eq. (3), $F_o \geq F_c$ always

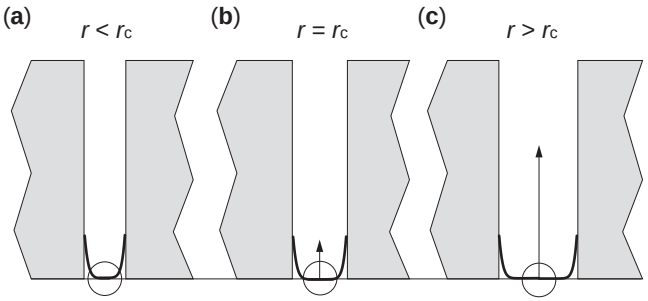

FIG. 4: Illustration of critical radius r_c. Bold curves are drawn from the steep wall potential as shown in Eq. (7). At $r < r_c$, the potential barrier and friction with respect to the solute particles is relatively high, which prevent the particle to transport through the channel. At $r \geq r_c$, the molecular friction provided by channel is relatively low, which allows the particles to have chance to transport through the channel.

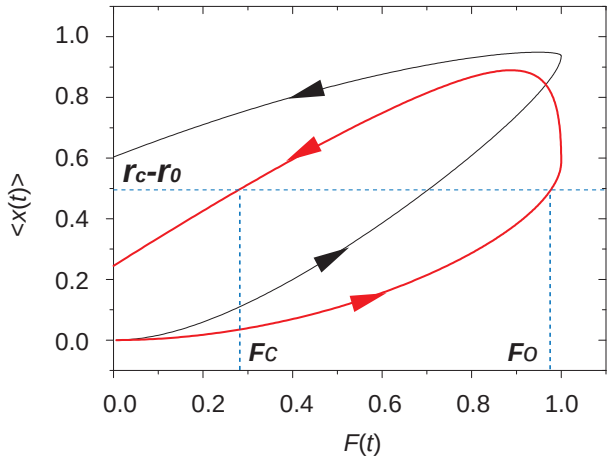

FIG. 5: (Color online) The critical radius determines two critical forces by hysteresis. Black curve shows a slow $F_+(t)$ ($\omega = 1/2$) coupled with fast $F_-(t)$ ($\omega = 2$). Red curve shows a fast $F_+(t)$ ($\omega = 2$) coupled with slow $F_-(t)$ ($\omega = 1/2$). Other parameter: $a = 2\pi\alpha = 6(\pi\beta)^{-1}$.

holds. Thus, for a periodic external driving force $F(t)a\sin(\omega t)$, the DNA channel can be opened when $F(t) > F_o$, and closed when $F(t) < F_c$, which relates the switching of DNA channel to its stochastic dynamics.

To provide an in-depth understanding to the critical forces, please note that in Fig. 5 the trajectory of DNA channel conformation is mean value over a large number of individual trajectories. A single trajectory without average treatment contains stochasticity originated from Gaussian noise and system fluctuation. Thus, a single real trajectory of DNA channel can result in different critical forces compared to those shown in Fig. 5. Actually, the critical forces determined in the mean trajectory of DNA channel should be understood as mean critical forces averaged from a large number of individual trajectories. If we have experimental method to measure the critical forces in single trajectory of DNA channel, the measured data should have indispensable fluctuation consistent to stochastic factors in Fokker-Plank equations.

IV. THE MEAN RESIDENCE NUMBER OF SOLUTE PARTICLE INSIDE THE CHANNEL

Before we can couple the channel gating with single-file transportation, the microscopic switching criticality should be related to macroscopic quantity. This problem is equivalent

to that how the different concentration gradient provide microscopic external force on the channel. The first step towards the solution is to clarify how many particles inside the channel at a time at given concentration gradient. Since the transmembrane pores have radii comparable to solute particles, we use a one-dimensional exclusion model to describe the single-file particle flows [2, 3, 4, 24]. Consider the nanopore shown in Fig. 6, with solute particles driven from left (inner) to right (external) by osmotic pressure of by hydrostatic pressure. A single-file channel is divided into M sections labeled i, each of length $l \gtrsim$ diameters of solute particles. The site of particle in the left reservoir is labeled $i = 0$, and that in the right reservoir is labeled $i = M+1$. The occupation of particles at site i is defined by $\tau_i \in \{0, 1\}$. The probability per unit time that a particle enters the channel from the left reservoir is $P_{01}dt$ if site $i = 1$ is unoccupied. Similarly, the probability that a particle gets out of the channel into left reservoir in time dt is $P_{10}dt$. As shown in Fig. 6, the entrance and exit probability for a particle in the right reservoir in time dt is similarly defined as $P_{M,M+1}dt$ and $P_{M+1,M}dt$. In the channel interior, solute particles move from site i to $i \pm 1$ with probability per unit time $P_{i,i\pm1}$ only if the adjacent site is unoccupied, i.e., $\tau_{i\pm1} = 0$. Under the approximation of a uniform and isotropic channel, we can simplify $P_{i,i\pm1}$ to P_c.

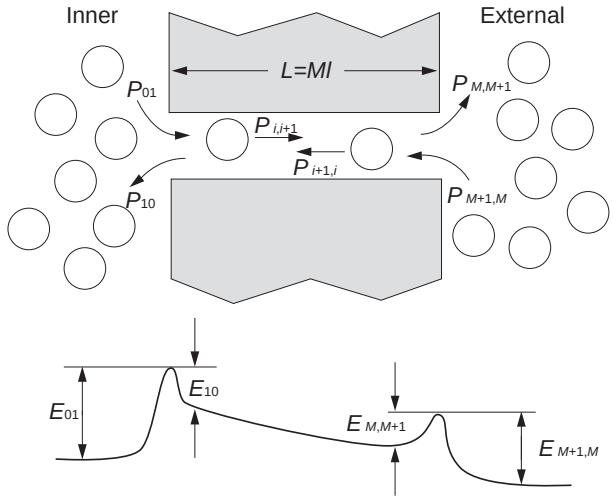

FIG. 6: Schematic drawing of osmosis and pressure driven flow through DNA channels separating inner reservoir of DNA nanocompartment and external infinite reservoir. The coefficients P_{01}, P_{10} ,$P_{M,M+1}$, and$P_{M+1,M}$ are conditional particle entrance and exit probabilities at channel ends. The coefficients $P_{i,i+1}$ and $P_{i+1,i}$ are hopping probabilities of particle along the one-dimensional channel. The bottom part of this figure depicts energy barriers for solute particles.

Microscopic thermodynamics in the channel-particle system involves three time scales. The first is the mean time between two adjacent events that a particle inside the channel collides with either the adjacent particles or the interior surface of the channel, defined as t_c. The second is the mean time that the absolute residence number of solute particles filled in the channel change its value one time, defined as t_n. And the third is the time scale over which we average the accurately simulated residence number of particles in the channel interior, defined as t_s. If we assume that local thermodynamic equilibrium (LTE) is satisfied in the system, the relation among the three time scales is $t_s \gg t_n \gg t_c$. In liquid phase osmosis across single nanopores where $J \leq 10^9/s$, typical pore diameters and interparticle spacing $\lambda \sim 5\mathring{A}$, and ambient thermal velocities $v_T \simeq 4 \times 10^4 cm/s$, yield collision times $t_c \simeq \lambda/v_T \simeq 1ps \ll J^{-1}$.

Based on LTE condition, the kinetic rates, P_{ij}, can be estimated from Arrhenius forms

$$P_c(n) \approx \frac{v_T}{l} e^{-E_c(n)/k_B T}, \tag{8}$$

$$P_{01}(n) \approx \frac{1}{4} c_i v_T \pi r^2 e^{-E_{01}(n)/k_B T}, \tag{9}$$

$$P_{M+1,M}(n) \approx \frac{1}{4} c_e v_T \pi r^2 e^{-E_{M+1,M}(n)/k_B T}, \tag{10}$$

$$P_{10}(n) \simeq \frac{v_T}{l} e^{-E_{10}(n)/k_B T}, \tag{11}$$

$$P_{M,M+1}(n) \simeq \frac{v_T}{l} e^{-E_{M,M+1}(n)/k_B T}, \tag{12}$$

where $v_T = \sqrt{\frac{k_B T}{m}}$ is the thermal velocity, l is the length of a channel section, r is the channel radius, c_i is the particle concentration at inner reservoir of DNA nanocompartment, c_e is the particle concentration at external reservoir, E_c, E_{01}, E_{10}, $E_{M+1,M}$, and $E_{M,M+1}$ are activation energies for solute particles to realize the corresponding position variation. For a soft nanochannel, which can change its conformation responding to the change of the mean residence number ($\overline{n}$) of particle in the channel interior, all the kinetic rates and corresponding activation energies are the functions of $\overline{n}$. For an illustrative example, we assume microscopically symmetric channel, i.e., $P_{01} = P_{M+1,M}$, and $P_{10} = P_{M,M+1}$.

To simulate and calculate the statistical quantity of mean residence number of particles inside a DNA channel as a function of concentration gradient applied on both sides of the channel, the first step is to count the number of microstates of the system and determine the transition probabilities between two adjacent states. The microstates are represented as $\{\tau_i\}(\tau_i \in \{0, 1\}, i \in [1, M]$, where τ_i is previously defined as the number of solute particle

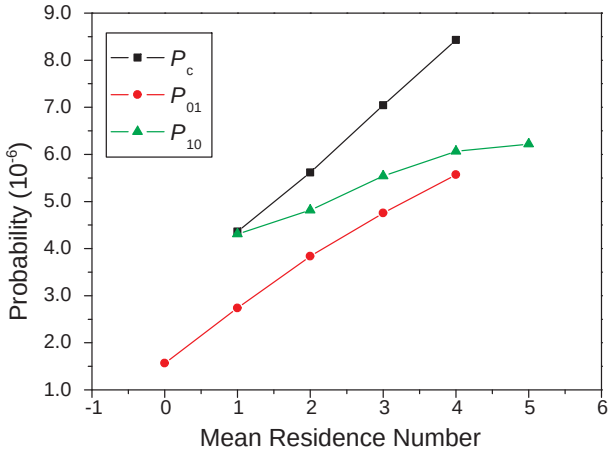

FIG. 7: (Color Online) The probabilities of entrance, exit, and hopping of particles as a function of the mean residence number, which are typically used in the simulation of Fig. 8.

occupying the ith section of the channel. The instantaneous number flux between section i and $i+1$ is

$$j_i(t) = P_{i,i+1}\tau_i(t)[1-\tau_{i+1}(t)] - P_{i+1,i}\tau_{i+1}(t)[1-\tau_i(t)]. \tag{13}$$

Note that $j_i(t) \in \{0, \pm 1\}$. The following expression is used to measure $\bar{n}$ in computer simulation program

$$\bar{n} = \frac{1}{T}\sum_{t=t_0}^{t_0+T} n(t), \tag{14}$$

where t is dimensionless time, t_0 is the time when the measurement begins, $n(t)$ is the particle number occupying in the channel interior at time t, T is the total time interval over which the measurement maintains.

The probabilities P_{ij} should change with the change of channel diameter when the channel are dilated by the particle filling in it. The change can be understood according to

$$\frac{\partial P_{ij}}{\partial \bar{n}} \approx -\frac{v_T\beta}{l}e^{-\beta E_{ij}}\left(\frac{\partial E_{ij}}{\partial r}\right)\left(\frac{\partial r}{\partial \bar{n}}\right). \tag{15}$$

Since $\frac{\partial E_{ij}}{\partial r} < 0$ and $\frac{\partial r}{\partial \bar{n}} > 0$, $\frac{\partial P_{ij}}{\partial \bar{n}} > 0$. The probabilities used in our simulations are accordingly shown in Fig. 7. The probability $P_{M,M+1}dt$ and $P_{M+1,M}dt$ are fixed at 10^{-8} order of magnitude, and independent of $\bar{n}$. Set t to be the dimensionless simulation time step. At t = 0, the temperature and concentrations is fixed at given value: $T = 300K$, c_i = 10 mM, c_e = 0.1 mM, and τ_i ($i \in [1, M]$) is set zero. Let solute particles to move randomly from one

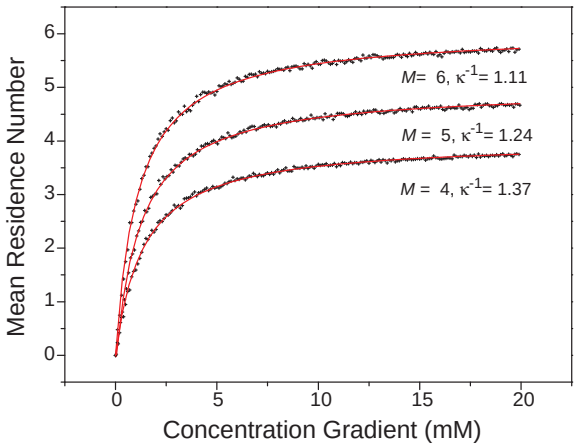

FIG. 8: (Color Online) The relation between the mean residence number and concentration gradient for three different length of the DNA channels. In the experimental system of DNA nanocompartment, specially designed dsDNAs have 15∼20 base-pairs and a 6∼7 nm double helix length. Comparing the channel length with the particle size, $M = 5$ typically reflects our experimental configurations.

site to its adjacent site, weighted by corresponding transition probability, if the adjacent site is not occupied. We set $t_c = 1$, then the time scale of filling number variation, t_n, would be in $10^3 \sim 10^4$ order of magnitude. Thus, the system will definitely achieve the equilibrium state and a stable distribution of particles after $t = 10^8$. After that, we measure the mean residence number in a time interval of $t_s = 10^9$, and thus obtain the simulated data. If a large amount of simulated data is obtained under the same condition, we find that the data obey a Gaussian distribution without obvious deviation.

The mean residence number $\bar{n}$ as a function of the concentration gradient is simulated, with temperature fixed at 300K. In the simulations, the concentration of solute particle in external solution is fixed at 0.1 mM, while the concentration in nanocompartment varies from 0 to 20 mM. Figure 8 shows the typical simulation results for the case of $M = 4, 5, 6$. The mean residence number under different concentration gradient can fit well to Langmuir isotherm. In Fig. 9, we further change the kinetic rates to test the effect on the simulations. It shows that the association constant in Langmuir isotherm does not change seriously at most cases. We observe that fluctuation in simulated data decrease seriously with increasing the entrance, exit, and hopping probabilities. In Figs. 9(c),(d),(e), the simulated data fit

fairly well to the Eq. (16) as shown below. The simulated Langmuir isotherms are well reasonable and theoretically expected. Actually, if LTE condition are well satisfied in a single-file channel system, the mean residence number should obey a single-site occupation mode, which mathematically is the same as single-site binding mode, i.e., first-order Langmuir isotherm. Using equilibrium statistical mechanics based on partition function weighted by binding energies of each site, one can exactly work out a first-order Langmuir isotherm relation between $\bar{n}$ and $C = c_i - c_e$, which is written as

$$\bar{n} = \left(\frac{C}{C + \kappa^{-1}} \right) n_m, \tag{16}$$

where κ is the association constant and n_m is the maximum mean residence number. And

$$\kappa^{-1} = \left(\frac{2\pi m}{\beta} \right)^{3/2} e^{-\beta \varepsilon_c}, \tag{17}$$

where β is Boltzmann constant, m is the mass of particles, and ε_c is effective site occupation energy for a particle.

To relate the microscopic switching criticality to macroscopic quantity, we consider that $F(t)$ only comes from the channel-particle interactions. It is reasonable to propose that $F(t)$ is related to the mean residence number $\bar{n}(t)$ of the particles inside the channel by a linear form

$$F \sim \bar{f} \bar{n}, \tag{18}$$

where $\bar{f}$ is the effective mean force of single particle exerted on the channel surface. The next step is to find the relation between $\bar{n}(t)$ and $C(t)$. The relation can be denoted by $\bar{n}(t) = \zeta(C(t))$. The real form of $\zeta(x)$ is dependent of the intrinsic properties of both channel and particle and their interactions. If the change of $C(t)$ in time scale t_s is enough small, the ζ-relations can be asymptotically adopted as Eq. (15). Since Eqs. (16) and (18) establish monotonically increasing functions between $F(t)$ and $C(t)$, the two critical forces (F_o, F_c) define two critical concentration $C(t)$ by

$$C^*_{o,c} = \zeta^{-1}(F_{o,c}/\bar{f}) \tag{19}$$

which characterizes the switching criticality through macroscopic quantity. If $\zeta(x)$ takes form of Langmuir isotherm, then

$$C^*_{o,c} = \left[\kappa \left(n_m \bar{f}/F_{o,c} - 1 \right) \right]^{-1}. \tag{20}$$

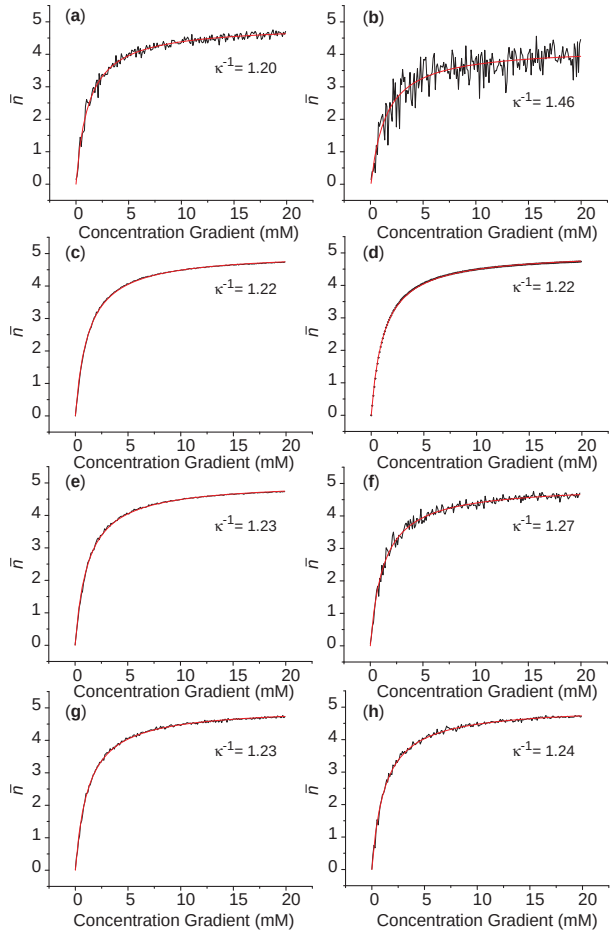

FIG. 9: (Color Online) The effect of the changes of probability on the simulated ζ-relations. (a) The data simulated on all probabilities shown in Fig. 7 times a factor 0.1. (b) The data simulated on all probabilities shown in Fig. 7 times a factor 0.01. (c) The data simulated on all probabilities shown in Fig. 7 times a factor 10. (d) The data simulated on all probabilities shown in Fig. 7 times a factor 100. (e) Only P_c times 10. (f) Only P_c times 0.1. (g) P_{01} and P_{10} times 10. (h) P_{01} and P_{10} times 0.1.

This formula establishes an important relation between microscopic critical condition with macroscopic condition, which provides a principle to control microscopic criticality through macroscopic experimental methods.

V. COUPLING OF CHANNEL GATING WITH SINGLE-FILE FLUX PUMPING

We consider how particles with a radius comparable to the radius of the channel transport through the dsDNA membrane in the viewpoint of time evolution. Given that the channel is in equilibrium state at time $t = 0$, the concentration difference of the particles on the two sides of a DNA channel increases along certain function $\Delta C(t)$ where $\Delta C(0) = 0$. The process of the flux establishment involves two stages according. In the first stage, $C(t) < C_o^*$, so that the particles have no sufficient chemical potential to transport through the channel. Even though the particles can penetrate into the channels, they are soon trapped in the channels without flux established. In the second stage, $C(t) > C_o^*$, and the concentration difference allows the particles trapped in the channels form a concerted motion to establish a transport flux. This Section is devoted to provide a mathematical description to the whole process, which is based on our recent experiments.

During the process, the channel will change its conformation from a closed state to an open state. This conformational transition can change the dynamics of single-filing particles transporting the pore. Reversely, the single-filing flux can also interact with channel to trigger conformational transition of the channel or maintain its conformational state. The dynamics of the system should involve both the channel and all particles transported. To show the dynamics of channels and particles in a coupling way, we notice that the Fokker-Plank equations describing the counterparts should be considered simultaneously rather than independently. This implies that the simulation study on ζ-relations is not enough, and we should further investigate the kinetic behavior of steady-state flux when channels are opened.

Single-file Brownian motion of solute particles along a narrow channel is in the over-damped limit of one-dimensional Langevin dynamics [5, 9, 38, 39, 40, 41, 42], described by the equation $\gamma\dot{x} = -U'(x)+\xi(t)$, where $-U'(x)$ is the potential of mean force [9] that guides the transport of particle through the channel, $\xi(t)$ is a Gaussian white noise with $\langle\xi(t)\rangle = 0$ and $\langle\xi(t)\xi(0)\rangle = 2D_p\gamma^2\delta(t)$. Here, $\delta(t)$ is the Dirac-delta function; D_p is the effective diffusion coefficient of a solute particle inside the channel, which related to γ through Einstein relation $D_p = k_BT/\gamma$ according to the fluctuation-dissipation theorem. The corresponding

FPE of this equation reads

$$\begin{aligned} &\partial_t p(x,t) = -\partial_x j(x,t), \\ &j(x,t) = -\tfrac{1}{\gamma}[\varepsilon \partial_x p(x,t) - U'(x)p(x,t)], \end{aligned} \tag{21}$$

where $\varepsilon = k_B T/m$. In the steady state, the flux is constant throughout the channel ($\partial_t p(x,t) = -\partial_x j(x,t) = 0$), we have [9, 38, 39, 40, 41, 42]

$$j(t) = A_1 C(t) - A_0 C_0, \tag{22}$$

where $A_i = \frac{\varepsilon}{\gamma} e^{U_i/\varepsilon} \left[\int_{x_1}^{x_2} e^{U(x)/\varepsilon} dx\right]^{-1}$, $i = 0, 1$, and $U_0 = U(x_2)$ and $U_1 = U(x_1)$. Therefore, when the channels are opened and steady state flux established, the change of $C(t)$ due to the steady state flux is

$$dC(t) = -j(t)N(t)V^{-1}dt, \tag{23}$$

where $N(t)$ is the total number of the open channels with flux established, and V is the volume of the reservoir in the nanocompartment. In the steady state, $N(t)$ does not explicitly depend on $C(t)$, but has a constraint of $\sum_{i=0}^{N(t)} \pi(r_i^2 - r_0^2) \leq \ell h$, where r_i is the radius of the ith open channel, ℓ is the edge circumference of the whole nanocompartment, and h is the height of the nanocompartment. This constraint indicates that the collective dilation of all open channels should not exceed the total area increase of the DNA membrane, which have a physical limit owing to the covalent binding on substrate surface.

To show how the single-file flux pumping is coupled with the channel gating, we suppose that $C(t)$ initiates from a value $C(t=0) = C_1 < C_o^*$ and, due to external particle supply, increases as a function of time $C(t) = C_{sm}(1 - e^{-t/\tau_s}) + C_1$ at $t < t_o$. This process can be experimentally realized by surface-based chemical reactions [45]. At $t = t_o$ where $C(t_o) = C_o^*$, the channels are activated from the closed state. As a result, $j(t)$ is established and $C(t)$ tends to decease according to Eq.(9) until $t = t_c$, where $C(t_c) = C_c^*$. At $t_o < t < t_c$, the particle source contributes to $dC(t)$ by $dC(t) = C_{sm}\tau_s^{-1} \exp(-t/\tau_s)dt$. Considering the other contribution described by Eq. (8), we obtain ordinary differential equation about $C(t)$

$$\frac{d}{dt}C(t) = C_{sm}\tau^{-1}e^{-t/\tau_s} - j(t)N(t)V^{-1}. \tag{24}$$

Inserting Eq. (7) into Eq. (9), we find the solution of $C(t)$ at interval $t_o < t < t_c$

$$C(t) = e^{-T(t)} \left\{ \int_{t_o}^{t} \left[\tfrac{C_{sm}}{\tau_s} e^{-\frac{t'}{\tau_s}} + \tfrac{A_0 C_0}{V} N(t')\right] e^{T(t')} dt' + C_0^* \right\}, \tag{25}$$

where $T(t) = \frac{A_1}{V}\int_{t_o}^{t} N(t')dt'$. After $t = t_c$, the channels are closed and flux is cut off. Note that in this analysis we have assumed that when the channel is switched on, the rate at which flux reaches to steady state is much larger than the rate at which steady state flux evolves with time [38]. To obtain an intuitive analysis, it is simple but instructive to select $N(t) = N_0$, and $\zeta(C) = \left(\frac{C}{C+\kappa^{-1}}\right) n_m$ (Langmuir isotherm), where κ is the association constant and n_m is the maximum of the mean residence number $\bar{n}(t)$. The Eq. (25) then is simplified to

$$C(t) = \frac{C_{sm}}{\tau_s - \tau_j} e^{-t/\tau_s} + (C_o^* - C' - \frac{C_{sm}\tau_j e^{-t_0/\tau_s}}{\tau_s - \tau_j}) e^{-(t-t_0)/\tau_j} + C', \tag{26}$$

where $\tau_j = V(A_1 N_0)^{-1}$, and $C' = A_0 C_0 A_1^{-1}$. Once $C(t)$ is determined, $j(t)$ can be easily determined from Eq. (22). Therefore, by coupling Eq. (26) with Eqs. (4) and (20), a typical complete dynamic process determined by hysteresis is numerically generated in Fig. 10. Figure 10(a) shows the time evolution of $C(t)$ and $j(t)$. Figure 10(b) exhibits how $r_c = r_0 + 0.56$ (nm) can cause $C_o^* = 18.32$ mM and $C_c^* = 3.29$ mM. This calculation fit well to the data from the experiments [45].

This numerical calculation can be more precise by using more accurate $C(t)$ and $N(t)$ functions, which can make the discontinuity of first-order derivative of $C(t)$, $j(t)$, and $\langle x(t)\rangle$ vs. $C(t)$ to become continuous at critical points. Typically, $N(t)$ can be refined by using the probability of channel opening, $P_o = \frac{1}{1+\exp(-\beta\Delta U_C)}$, where ΔU_C is the change of deformation energy during the channel opening [1, 47, 48]. However, the main features will not change under these detailed improvements. While current experimental techniques are far away from observation on the detailed dynamics, we do not work much further on these improvements. Theoretically, these improvements can not essentially promote the quality of this study.

The general calculation method used to couple the gating of soft nanochannel with single-file flux pumping of solute particles can be summarized as following procedures:

(1) To estimate the critical radius of channel switching from the channel radius and particle sizes;

(2) To find the increasing phase of the concentration gradient across the channel;

(3) To determine the opening critical concentration gradient according to critical radius by solving the Eq. (4) of the soft nanochannel dynamics corresponding to the increasing phase of the concentration gradient;

(4) To find the decreasing phase of the concentration gradient across the channel;

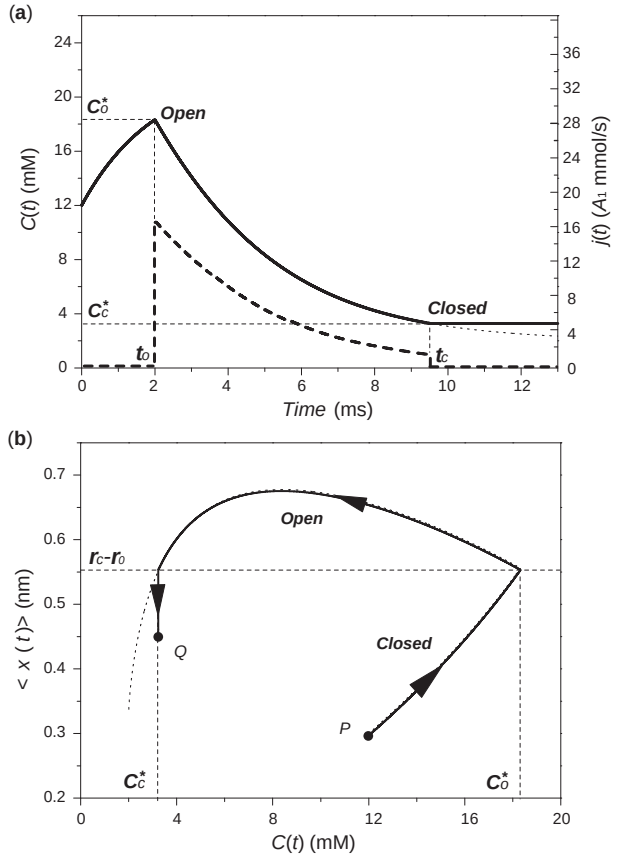

FIG. 10: Coupling of channel gating with flux pumping. Bold solid line shows the time evolution of $C(t)$, and bold dashed line shows the time evolution of $j(t)$. Unit of $j(t)$ is scaled to the value of A_1. (Inset) The mean trajectory of channel conformation changed with $C(t)$ in the dynamic evolution (start from P and stop at Q), showing how the switching radius r_c determines the dual critical value $C^*_{o,c}$ by hysteresis. The parameters used are based on experiments shown in Fig. 4: $C_{sm} = 10$ mM, $C_1 = 12$ mM $A_0C_0(A_1)^{-1} = 2$ mM, $\tau_s = 2$ ms, $V(A_1N_0)^{-1} = 2.5$ ms, $D_p \sim 10^8$ Å s^{-1}, $h = 5$ nm, $\kappa = 250$ M^{-1}, $2\pi\alpha\beta D = 0.036$ s^{-1}, $\bar{f}n_m\beta D = 0.036$ m s^{-1}.

(5) To determine the closing critical concentration gradient according to critical radius by solving the Eq. (4) of the soft nanochannel dynamics corresponding to the decreasing phase of the concentration gradient.

In the numerical calculation, we neglect some intrinsic complexity that is not important for the points studied here. First, we do not take into account the defects as an important affection to the macroscopic effects. In a real surface of ADNC device, random microstructure or even nanostructure may contribute specific effect. Experiments showed that this effect is

on the continuous small decrease of measured $C(t)$, which does not affect the pumping effect during a whole switching process that experimentally results in a steep drop in $C(t)$. Second, the microscopic behavior of molecules inside nanocompartment may be very different from those in the bulk solution. Although we never add this effect due to its elusiveness and still under investigation, this deficiency does not affect the major character of the transport mechanism described here, and also does not contribute specific effect on experiments.

VI. DISCUSSION AND SUMMARY

This study starts from the microscopic thermodynamics of single DNA channels and ends at coupling of channel gating with single-file flux pumping. Although the theoretical modeling includes a few coarse-graining treatment, we have established a minimal model to unify the channel gating and single-file flux pumping into one picture. The model is further verified by our recent experiments [45]. While being put into simplicity, there can be several ways to improve and enrich this picture. For example, we can further ask whether the asymmetry of DNA channel during its gating could contribute nontrivial effect on the single-file transport, whether the critical radius shifts according to the concentration gradient, and so on. One would notice that these questions can raise nontrivial tasks to find right answers. So they remain for the future studies.

In Section IV, the simulated isotherms for the mean residence number $\bar{n}$ of solute particle inside a channel seem to have trivial results that fit to Lamguir isotherm, which can be exactly derived from equilibrium statistical mechanics. However, our simulation is not based on equilibrium statistical mechanics, but one-dimensional exclusion transport model, which is typically nonequilibrium transport. Therefore, an interesting conclusion can be made, that if measurement on $\bar{n}$ does not distinguish the difference between individual particles, the $\bar{n}$ averaging over a time interval that is wide enough on the steady-state flux of a one-dimensional nonequilibrium transport is equivalent to static occupation of equilibrium particles along the channel. Another reason for this conclusion is that during the measurement of $\bar{n}$ isotherms, the roles of the left and right reservoirs are the same, so that their exchange of particle with channel can be treated as a whole, which results in that steady-state flux is equivalent to zero net exchange number between channel and the reservoirs as a whole. This conclusion also shows the reasonability of applying a equilibrium statistical

mechanical method on the mathematical derivation of $\bar{n}$ isotherms. This can also explain why the changes of probabilities of entrance, exit, and hopping of particles relative to the channel do not seriously affect the simulated association constant.

Although focusing on the case of DNA-formed nanochannels, we emphasize that the nonequilibrium single-file pumping dynamics investigated here is not limited to this case, which provides a general framework to describe the dynamics of many other soft nanochannels. First, similar gating thermodynamics is also adopted by mechanosensitive protein channels [25, 35]. Second, the fundamental behavior of single-file penetration isotherms and flux hysteresis simulated do not highly rely on the specific properties of DNA. Third, Some of its modeling also have direct implication for other nanochannels. Even though the mechanosensitive protein channels [49] have various detailed gating mechanism [30, 34, 35, 36, 37], these studies most neglect the flexibility of channels and do not exclude out the effect of the flexibility on the channel gating dynamics. Therefore, this study is well complementary to current studies on protein channel gating and transportation [2, 3, 4, 11, 12, 25, 30, 31, 32, 33, 34, 35, 36, 37, 38, 39, 40, 41, 42, 43, 44, 51, 52], as well as non-soft molecular sieves [6, 7, 8, 11].

The main idea of this study is that by dynamic hysteresis one microscopic critical condition leads to dual criticality corresponding to the conjugate segments of the time evolution trajectory in the regime far away from thermodynamic equilibrium states, which can be represented by both microscopic and macroscopic quantities. Fluctuation theorem (FT) [50] have shown that the probability density function $\pi(s_\tau)$ of a phase space trajectory is deviated from its time reversal trajectory $\pi(-s_\tau)$ by relations typically like $\pi(s_\tau)/\pi(-s_\tau) = \exp(\tau s_\tau)$, where s_τ is the entropy production rate. It is also valid for stochastic dynamics [53, 54, 55] that can describe many biological and nano-mechanical systems. It was further shown that the transient fluctuation theorem are in quantitative agreements with Langevin dynamics [56]. Note that it is Langevin dynamics causing the hysteresis during the switching of soft channels. Since the origin of dynamic hysteresis is in the same principle of FT, our dual criticality model may find widespread valid variations in other biological and nanometer systems, e.g., protein channels and soft molecular sieves.

This work was supported partly by the Ministry of Science and Technology of P. R. China, Peking University, and National Center for Nanoscience and Technology.

[1] B. Hille, *Ion Channels of Excitable Membranes* (Sinauer Associates, Sunderland, MA 2001).

[2] T. Chou, Phys. Rev. Lett. **80**, 85 (1998); J. Chem. Phys. **110**, 606 (1999).

[3] T. Chou, J. Chem. Phys. **110**, 606 (1999).

[4] T. Chou and D. Lohse, Phys. Rev. Lett. **82**, 3552 (1999).

[5] M. Kollmann, Phys. Rev. Lett. **90**, 180602 (2003).

[6] G. Hummer, J. C. Rasaish and J. P. Noworyta, Nature (London) **414**, 188 (2001).

[7] A. Berezhkovskii and G. Hummer, Phys. Rev. Lett. **89**, 064503 (2002).

[8] A. Kalra, S. Garde and G. Hummer, Proc. Natl. Acad. Sci. USA **100**, 10175 (2003).

[9] I. Kosztin and K. Schulten, Phys. Rev. Lett. **93**, 238102 (2004).

[10] M. Ø. Jensen, S. Park, E. Tajkhorshid,and K. Schulten, Proc. Natl. Acad. Sci. USA **99**, 6731 (2002).

[11] D. S. Sholl and K. A. Fichthorn, Phys. Rev. Lett. **79**, 3569 (1997).

[12] F. Zhu, E. Tajkhorshid, and K. Schulten, Phys. Rev. Lett. **93**, 224501 (2004).

[13] N. C. Seeman, Nature (London) **421**, 427 (2003).

[14] B. Samori, G. Zuccheri, Angew. Chem. Int. Ed. **44**, 1166 (2005).

[15] P. W. K. Rothemund, Nature (London) **440**, 297 (2006).

[16] C. Mao, W. Sun, Z. Shen, and N. C. Seeman, Nature (London) **397**, 144 (1999).

[17] B. Yurke, A. J. Turberfield, A. P. Mills Jr, F. C. Simmel, and J. L. Neumann, Nature **406**, 605 (2000).

[18] H. Yan, S. H. Park, G. Finkelstein, J. H. Reif, and T. H. LaBean, Science **301**, 1882 (2003).

[19] K. Keren, R. S. Berman, E. Buchstab, U. Sivan, and E. Braun, Science **302**, 1380 (2003).

[20] Y. Mao, C. Luo and Q. Ouyang, Nucleic Acids Res. **31**, e108 (2003).

[21] Y. Mao, et al. Nucleic Acids Res. **32**, e144 (2004).

[22] S. A. Safran, *Statistical Thermodynamics of Surfaces, Interfaces and Membranes* (Perseus, Cambridge, MA, 1994).

[23] H. Risken, *The Fokker-Planck Equation* (Springer-Verlag Berlin Heidelberg 1989).

[24] B. Derrida, Phys. Rep. **301**, 65 (1998).

[25] V. S. Markin and F. Sachs, Phys. Biol. **1**, 110 (2004).

[26] A. A. Kornyshev and S. Leikin, J. Chem. Phys. **107**, 3656 (1997).

[27] A. A. Kornyshev and S. Leikin, Phys. Rev. Lett. **82**, 4138 (1999).

[28] A. A. Kornyshev and S. Leikin, Phys. Rev. Lett. **84**, 2537 (2000).

[29] A. A. Kornyshev and S. Leikin, Phys. Rev. Lett. **86**, 3666 (1999).

[30] M. S. Turner and P. Sens, Phys. Rev. Lett. **93**, 118103(2004).

[31] J. Zhang, A. Kamenev, and B. I. Shklovskii, Phys. Rev. Lett. **93**, 148101 (2005).

[32] K. Hahn,J. Kärger, and V. Kukla, Phys. Rev. Lett. **76**, 2762 (1996).

[33] B. Nadler, Z. Schuss, and A. Singer, Phys. Rev. Lett.**93**, 238102 (2005).

[34] I. Goychuk, and P. Hanggi, Proc. Natl. Acad. Sci. USA **99**, 3552 (2002).

[35] P. Wiggins, and R. Phillops, Proc. Natl. Acad. Sci. USA **101**, 4071 (2004).

[36] A. M. J. VanDongen, Proc. Natl. Acad. Sci. USA **101**, 3248 (2004).

[37] M. Grabe, H. Lecar, Y. N. Jan, and L. Y. Jan, Proc. Natl. Acad. Sci. USA **101**, 17640 (2004);.

[38] R. S. Eisenberg, M. M. Klosek, and Z. Schuss, J. Chem. Phys. **102**, 1767 (1995).

[39] A. Singer, Z. Schuss, B. Nadler, and R. S. Eisenberg, Phys. Rev. E **70**, 061106 (2004).

[40] A. Singer, and Z. Schuss, Phys. Rev. E **71**, 026115 (2005).

[41] B. Nadler, Z. Schuss, U. Hollerbach, and R. S. Eisenberg, Phys. Rev. E **70**, 051912 (2004).

[42] J. Piasecki, R. J. Allen, and J. P. Hansen, Phys. Rev. E **70**, 021105 (2004).

[43] L. Xu, M. G. Sedigh, M. Sahimi, and T. T. Tsotsis, Phys. Rev. Lett. **80**, 3511 (1998).

[44] X. Xia, and R. J. Silbey, Phys. Rev. E **72**, 085423 (2005).

[45] Y. Mao, S. Chang, S. Yang, Q. Ouyang, and L. Jiang. (to be published).

[46] J. E. Shea, and I. Oppenheim, J. Chem. Phys. **100**, 19035 (1996).

[47] R. Erdem, and C. Ekiz, Physica A **349**, 283 (2005).

[48] R. Erdem, and C. Ekiz, Physica A **351**, 417 (2005).

[49] P. G. Gillespie, and R. G. Walker, Nature (London) **413**, 194 (2001).

[50] D. J. Evans and D. J. Searles, Adv. Phys. **51**, 1529 (2002).

[51] B. Roux, Biophys. J. **77**, 139 (1999).

[52] O. Beckstein and M. S. P. Sansom, Phys. Biol. **1**, 42 (2004).

[53] J. Kurchan, J. Phys. A **31**, 3719 (1998).

[54] J. L. Lebowitz and H. Spohn, J. Stat. Phys. **95**, 333 (1999).

[55] D. J. Searles and D. J. Evans, Phys. Rev. E **60**, 159 (1999).

[56] D. M. Carberry, J. C. Reid, G. M. Wang, E. M. Sevick, D. J. Searles, and D. J. Evans, Phys. Rev. Lett. **92**, 140601 (2004).